Palaeogeography, Palaeoclimatology, Palaeoecology 675 (2025) 113090

Contents lists available at ScienceDirect

Palaeogeography, Palaeoclimatology, Palaeoecology

journal homepage: www.elsevier.com/locate/palaeo

Intense tropical cyclone activity over the past 2000 years at Bay of Islands, Fiji

Yanan Li [a,b,c,*], Jeffrey P. Donnelly [b], Nicole d'Entremont [b], James F. Bramante [b], Krishna K. Kotra [d], Shu Gao [a]

[a] *Ministry of Education Key Laboratory for Coast and Island Development, School of Geography and Ocean Science, Nanjing University, Nanjing, China*
[b] *Coastal Systems Group, Department of Geology and Geophysics, Woods Hole Oceanographic Institution, Woods Hole, MA, USA*
[c] *State Key Laboratory of Estuarine and Coastal Research, School of Marine Sciences, East China Normal University, 500 Dongchuan Rd., Shanghai 200241, China*
[d] *School of Agriculture, Geography, Environment, Ocean and Natural Sciences (SAGEONS), The University of the South Pacific, Emalus Campus, Port Vila, Vanuatu*

A R T I C L E I N F O

Editor: Amy Prendergast

Keywords:
Tropical cyclone
Reconstruction
South Pacific Convergence Zone
ENSO
Little Ice Age

A B S T R A C T

Tropical cyclones (TCs) are among the most devastating hazards, causing damage and fatalities in coastal communities. Our understanding of the climatic factors that modulate tropical cyclone activity is impeded by the short historical records and the scarcity of paleoclimatic reconstructions, with a notable dearth of data in the Southern Pacific region. In this paper, we present a sedimentary record from a coastal karst basin in Bay of Islands, Vanua Balavu, Fiji to provide insight into the regional intense TC activity over the past two millennia. A total of 53 intense storm events captured by this site are identified using coarse fraction (>63 μm) anomalies in sediment core retrieved from the basin, yielding an overall average event frequency of 2.6 events/century. Multiple centennial-scale quiescent periods (from 200 to 300 CE and 1000 to 1150 CE) and active periods (namely from 350 to 750 CE, 900 to 1000 CE, 1150 to 1250 CE, 1400 to 1500 CE, and 1650 to 2017 CE) are found in the reconstruction, and the most active interval spans from 1650 to 1800 CE at 4.5 events/century.

A comparison between existing paleostorm records and climate forcing indices suggests that the southward displacement of the South Pacific Convergence Zone (SPCZ) during the Little Ice Age with more La Niña events is responsible for the basin-wide increasing of tropical cyclone activity in the South Pacific. Decline of TC occurrence in the western SP during the Medieval Climate Anomaly is attributed to the northward movement of SPCZ. However, event frequency peaks of the latitudinally aligned sites in the South Pacific exhibit a certain degree of asynchrony, necessitating the acquisition of more detailed high-resolution paleostorm reconstructions within these basins and corroborative evidence from global climate models.

1. Introduction

Tropical cyclones (TCs) are among the most devastating hazards to coastal populations and property. Coastal morphology and ecosystems can be significantly reshaped, temporarily or irreversibly, by the hydrodynamic and sedimentological processes resulting from TC-induced wind, precipitation, surge, and waves. Given the potential of current climate warming to influence TC activity, gaining a better understanding of how TC activity varies with climate is key to assessing the risks to coastal populations and property.

Although the short duration of instrumental records has impeded the attempt of revealing multidecadal and greater patterns in TC activity, event deposits preserved in sedimentary archives provide proxies to reconstruct TC activities on longer timescales. Among various coastal sedimentary environments, coastal lakes and karst basins have relative quiescent hydrodynamic conditions in normal weather, while extreme waves and currents transport coarse grained sediments into the basin thus preserving a sedimentary record of the events since sediment accumulations in the deep basins are below wave base. The pioneering work of Emery (1969) recovered sandy tropical cyclone event beds from Oyster Pond, Massachusetts, US. After that, numerous centennial to millennial storm time series have been recovered using sedimentary archives from coastal lagoons, lakes, ponds and blue holes along the western North Atlantic Ocean (WNA) margins, the Gulf of Mexico and

* Corresponding author at: Ministry of Education Key Laboratory for Coast and Island Development, School of Geography and Ocean Science, Nanjing University, Nanjing, China.
E-mail address: yananli.nju@gmail.com (Y. Li).

https://doi.org/10.1016/j.palaeo.2025.113090
Received 6 October 2024; Received in revised form 29 April 2025; Accepted 9 June 2025
Available online 10 June 2025

Caribbean Sea (Liu and Fearn, 1993; Liu and Fearn, 2000; Donnelly et al., 2001a; Donnelly et al., 2001b; Donnelly, 2005; Donnelly and Woodruff, 2007; Brandon et al., 2013; Denommee et al., 2014; Wallace et al., 2014; Donnelly et al., 2015; Wallace et al., 2019, 2021), followed by the western North Pacific (WNP) as another hotspot region (Huang, 2000; Liu et al., 2001; Yu et al., 2009; Williams et al., 2016; Yue et al., 2019; Zhou et al., 2019; Yang et al., 2022; Tan et al., 2023).

The South Pacific (SP) is one of the main TC development regions. Toomey et al. (2013) retrieved a back-reef lagoon sedimentary record from Tahaa, French Polynesia and recovered a 5000-years TC occurrence series using coarse-grained event beds. They found that TC activity was more active from 3000 BCE to 1800 BCE and 1000 BCE to 1450 CE, which was suggested to be associated with the El Niño–Southern Oscillation (ENSO). Denniston et al. (2015) presented a 2200-year long record of cave flooding events from the northwest Australia, which was interpreted to be predominantly dominated by TC activity. They posited that the multi-centennial variability in extreme rainfall (increased rates in 50–400 CE, 850–1450 CE, and the twentieth century, and reduced occurrence in 500–850 CE and 1460–1650 CE) was driven by ENSO. Fitzsimons and Howarth (2022) reported a 10-ka flood frequency proxy from rapidly deposited layers preserved in lake sediments in the South Island, New Zealand. They related this proxy to TC activity but suggested the centennial to millennial active/quiescent climate states were mostly influenced by the strength of westerly airflow. Other reconstructions based on coral blocks, boulders and beach ridges are discontinuous but provide evidence of past TC occurrences (Hayne and Chappell, 2001; Nott, 2006; Forsyth et al., 2010, 2012; Yu et al., 2012).

Despite of the above studies in the SP basin, there is still a sparsity of continuous sediment TC proxy records compared to WNP and WNA. In the context of global warming and sea-level rise, low lying island countries in the Pacific are particularly vulnerable (Gooley et al., 2014), necessitating more centennial to millennial paleostorm reconstructions to further illuminate characteristics of regional TC activity, and to explore any underlying climate forcings. In fact, the depositional settings on numerous widely scattered volcanic and coral islands within the SP basin are well suited to develop TC reconstructions.

In this paper, we reconstruct a 2000-year record of TC activity for the central SP by identifying TC event layers from a coastal karst basin on

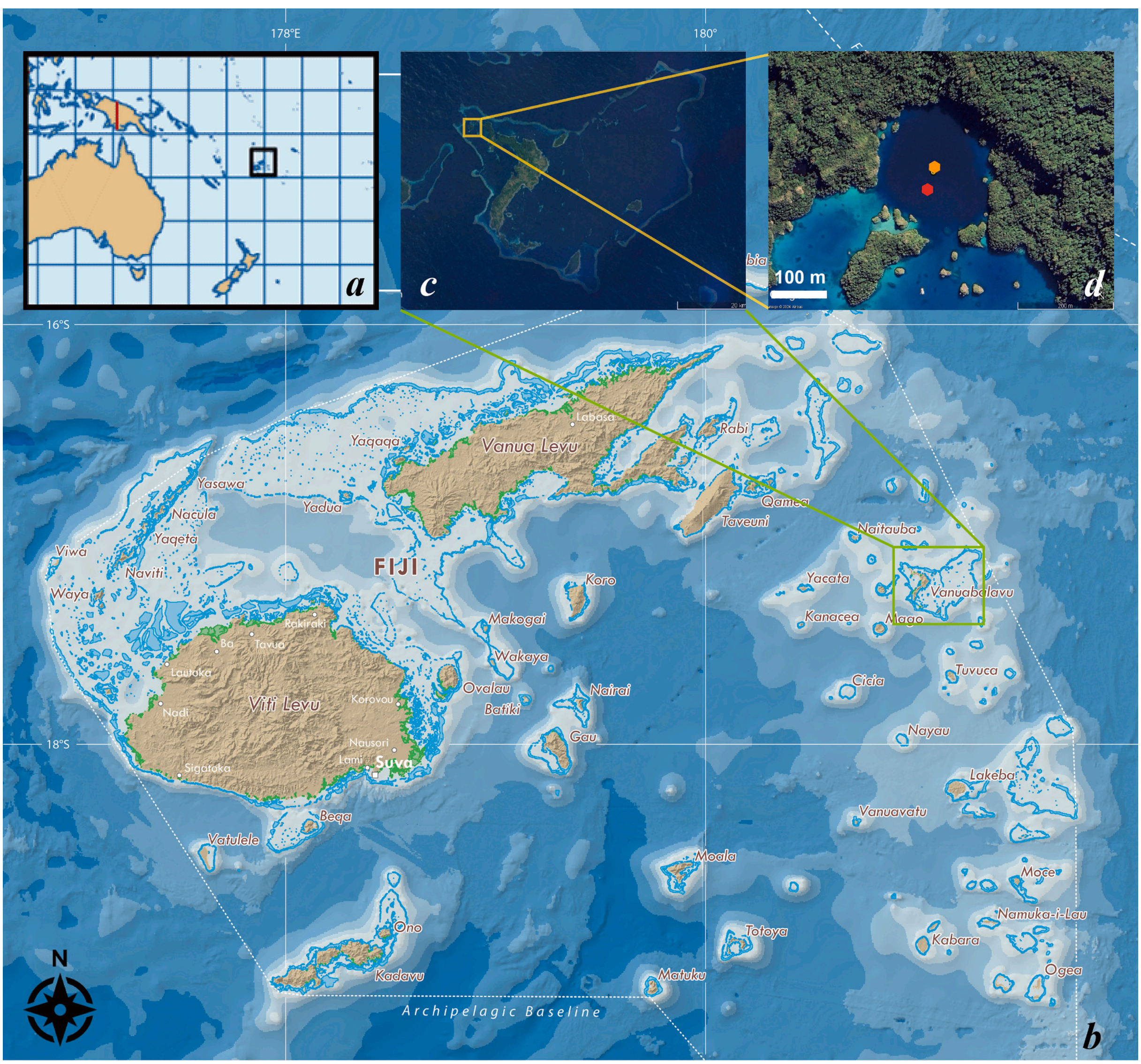

Fig. 1. Overview of the study site. (*a*) Fiji in the South Pacific; (*b*) Major islands of Fiji (modified from Gassner et al., 2019); (*c*) The Vanua Balavu Island (image source: Google Earth™); (*d*) The karst basin in the Bay of Islands, northwest of Vanua Balavu Island, where the orange and red dots respectively indicate the position collecting core BOI1 (17°10′28.80“S, 179° 0′55.20”W, water depth 33.0 m) and BOI2 (17°10′28.32“S, 179° 0′54.30”W, water depth 31.5 m) (image source: Google Earth™). (For interpretation of the references to colour in this figure legend, the reader is referred to the web version of this article.)

Vanua Balavu Island, Fiji. We compare this record to other TC and paleoclimate reconstructions in the SP basin and the Southern Hemisphere to investigate the coherency between existing records across the basin and to explore the dominating climate parameters.

2. Study site and methodology

2.1. Study site and field methods

The archipelago of Fiji is the subaerially exposed parts of Lau-Colville Ridge, the remnant arc of the boundary between the Pacific and Australian plates (Gill, 1976). It comprises some 350 islands, of which approximately 110 are permanently or temporarily inhabited. The two largest islands are Viti Levu and Vanua Levu (Fig. 1*b*), with the Lau group located to their east (Kumar, 2005; Neall and Trewick, 2008).

The Lau group islands exhibit a variety of lithologies and ages: their volcanic basements date from 5.5 Ma to 0.28 Ma, and the volcanic rocks are covered by reef limestone hundreds of meters thick (Nunn et al., 2002). Vanua Balavu is the largest island in the northern Lau group, and it lies with six other small islands within a very large barrier reef (Fig. 1*c*). The island is a Miocene-Pliocene volcanic complex, of which the central portion and the southern quarter are covered by volcanic rocks predominantly of basic composition, while a large area of coralline limestone accounts for the northern land surface area. Although the northern limestone landscape is generally gently rolling and basin-shaped, limestone outcrops and surface boulders are commonly found. The island is mostly covered by rainforests, while mangrove swamps dominate the western coastline as a narrow strip (Leslie and Blakemore, 1985).

At the coastal margins of northern Vanua Balavu, the limestone is cliff-like, with near-vertical rock faces pitted by karst effect (Leslie and Blakemore, 1985). A coastal karst basin we focus on here is located in the northwest coast of the island (Fig. 1*d*), which is approximately 300 m in diameter and 32 m in water depth. The basin connects to the adjacent lagoon water (named Bay of Islands) through two broad and shallow (< 2 m water depth) openings across reef flat to the south and southwest and is sheltered by a few islets. The lagoon bed consists of unconsolidated biogenic carbonate mud, sand and shell fragments and a veneer of sand to gravel sized sediments is on the reef flat. Sea-level reconstruction of the northeast Fiji suggests that the modern geomorphic settings of the reef barrier, reef flat, lagoon and karst basin were established at 2000 BCE – 1000 BCE (Nunn et al., 2002).

In November 2017, two cores (BOI1 and BOI2; see Fig. 1*d* for more details) were collected with a percussion corer from a portable raft. Water depth was measured with a handheld depthometer before coring. The water-sediment surfaces were recovered and preserved in the top sections.

Fiji's climate is maritime, dominated by the effects of the southeast trade winds, which create wet, cooler windward and dry, warmer leeward areas. November to April is recognized as the TC season (Leslie and Blakemore, 1985; Kumar, 2005) with a 2.8 annual TC number on average affecting the country, while TC numbers vary from 0 to 7 per season (PACCSAP, 2015) (see the Fig. S1 for TC impacting Fiji in the past 20 years). The coasts of Fiji mostly fall into microtidal category; waves in the region are influenced by the southern trade winds and the South Pacific Convergence Zone (SPCZ), and typically come from the east or southeast with mean wave heights of about 1.3 m (PACCSAP, 2015).

2.2. Sediment analysis

The cores, BOI1 and BOI2, were sectioned after recovery and transported to the Woods Hole Oceanographic Institution (WHOI). In the Coastal Research Laboratory (CRL) of WHOI, cores were split, described and sampled contiguously at 1 cm intervals. Each sample was dried overnight at 110 °C to determine its dry weight, and was wet screened through a 63 μm standard sieve to retain sand sized and coarser grains. The coarse grains were dried at 100 °C and weighed to calculate the coarse fraction.

2.3. TC event bed identification

Event beds in BOI cores can be visually discernable when they have abrupt contacts with underlying sediments, contain coarse grains such as quartz sands, carbonate sands and shell fragments. We use coarse fraction anomaly (>63 μm) as the means of characterizing coarse deposits downcore. A coarse fraction cutoff was determined for constituting event beds in BOI2 following the approach by Donnelly et al. (2015). Firstly, a baseline of 11-point moving average of coarse fraction values was generated, with major peaks (coarse fraction exceeding 5 %) excluded to prevent them from shadowing adjacent minor peaks. Then we smoothed out the decadal variability in the coarse fraction by deducting this baseline, and the differences were named coarse anomalies. After different cutoff thresholds were tested (see the Fig. S2 for more details), an event was defined as a peak that exceeds 1.3-σ of the cumulative distribution of the BOI2 coarse anomaly series.

2.4. Age control

Five terrestrial plant macrofossils were recovered from the core and were radiocarbon dated at the National Ocean Science Accelerator Mass Spectrometer (NOSAMS) facility at WHOI (dating results are found in Table S1). From the BOI2 top surface to 50 cm depth, 27 samples were collected at 1 cm interval to measure ^{210}Pb and ^{137}Cs activity (more details are provided in the Fig. S3).

Then the *Bacon* software (v2.3.5) (Blaauw and Christen, 2011) was used to derive a probabilistic age-depth model for BOI2 record, wherein the dating results were calibrated with SHCal13 (Hogg et al., 2013) for secular atmospheric radiocarbon concentration changes, and the depths of radiocarbon samples in the core were corrected.

An age-depth model was established for BOI2 core from radiometric dating results. Due to the disturbance of TC beds at the top of the core and resultant errors, the radiometric results of ^{210}Pb and ^{137}Cs were not adopted in the age model, but were used for cross-check purpose after the model were produced.

2.5. TC frequency calculation

Using the age-depth model for BOI2 and the event beds we identified, we created TC time series and calculated TC frequency (event per century) following the approach by Lane et al. (2011). This involved applying a 100-year sliding window through the event data, counting the number of TC events within the window, and taking this number as TC frequency. This centennial frequency can be compared with other centenary scale TC frequency records and paleo-climatological proxy reconstructions.

3. Results

3.1. Core description

The BOI2 core is slightly longer than BOI1 (Fig. S4) and they show very similar lithofacies, both featuring light tan colored (Munsell colour 5Y 9/2) silt and mud from top to bottom (Fig. 2*b*), with scattered shell fragments and plant debris. No laminations or discernable event beds were visually observed and no evidence of bioturbation was detected.

Coarse fractions (>63 μm) of the two cores range from 2 % to 10 %, and their major peaks match well (Fig. S4). The coarse fractions slightly increase above 180 cm in BOI2.

3.2. Event frequency variability

Only the samples from BOI2 were radiocarbon-dated. Radiometric

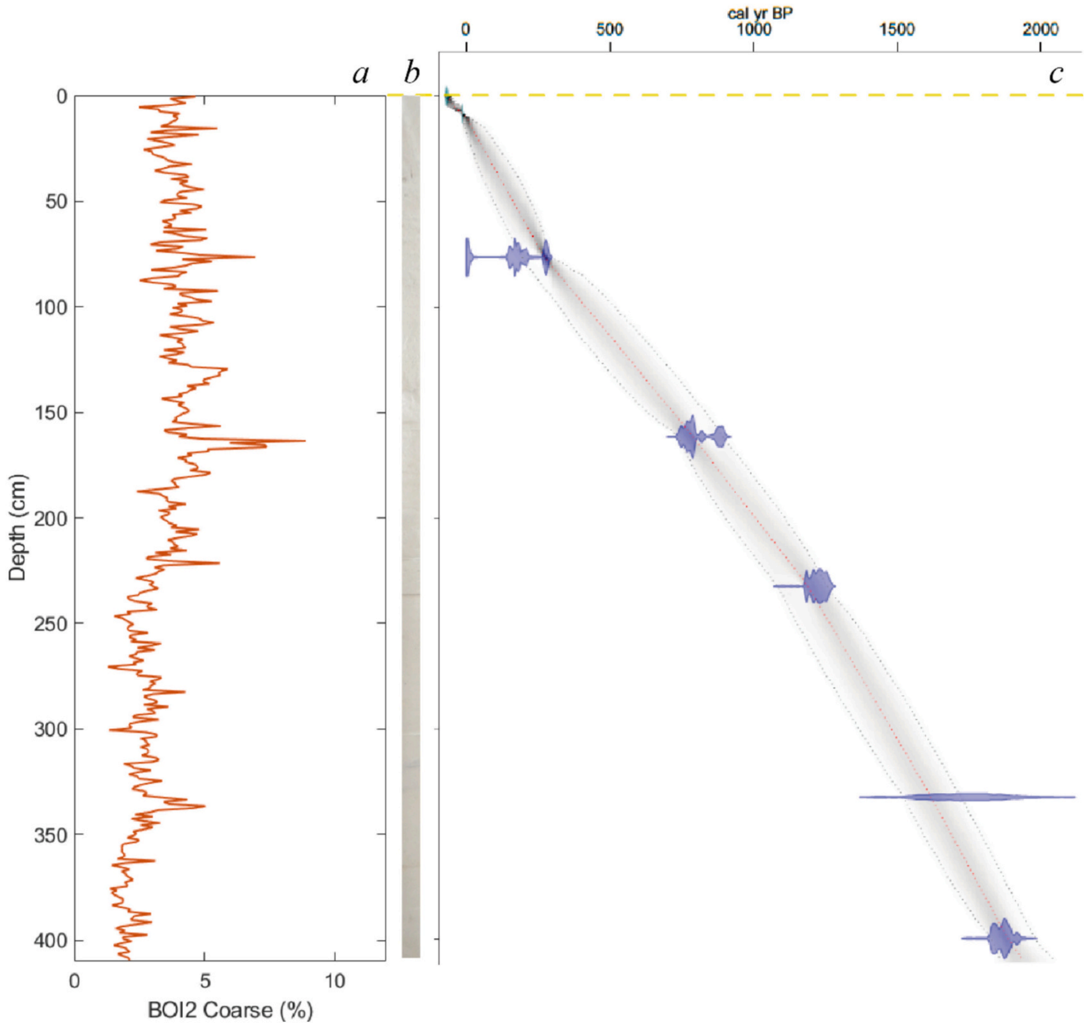

Fig. 2. Overview of the BOI2 core. (a) Coarse grain (>63 μm) fractions, (*b*) optical photo, and (*c*) age-depth model.

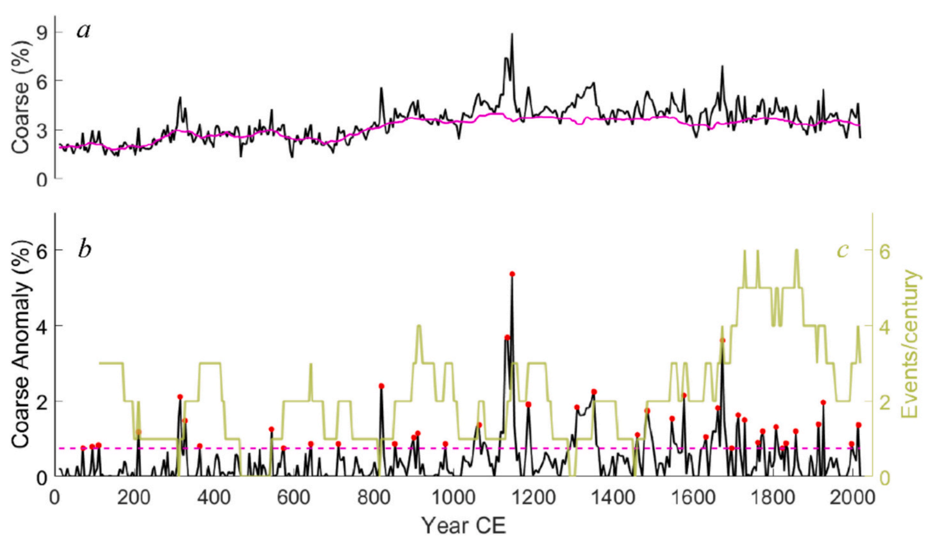

Fig. 3. Identifying TC events from coarse grain (>63 μm) anomalies and calculating event frequency. (*a*) Filtering out decadal variability of coarse grain by establishing a baseline (magenta line) of 11-point moving averages; (*b*) TC events (red stars) identified, with the magenta dashed line indicating the cutoff threshold; and (*c*) Event frequency in terms of event number per century. (For interpretation of the references to colour in this figure legend, the reader is referred to the web version of this article.)

dating results present almost-perfect chrono-stratigraphy order and yield an age-depth model back to 17 CE (Fig. 2c), indicating a very constant deposition rate (approximately 2 mm/year) in the karst basin. An approximate rate can be estimated from the ^{210}Pb dating results, while the 137Cs results are not available. Given the sampling interval of 1 cm, each sample represents approximately 5 years' worth of deposition.

In the past 2000 years, BOI2 has captured 42 storm events with 1.3-σ cutoff threshold used(Fig. 3b), and the resultant overall average event frequency is 2.1 events/century (Fig. 5e). This event frequency series also presents evidence of centennial active and quiescent periods. The five active periods were approximate from 350 to 750 CE, 900 to 1000 CE, 1150 to 1250 CE, 1400 to 1500 CE, and 1650 to 2017 CE. Among them, the most active time interval spanned from 1650 to 1800 CE at 4.5 events/century, remarkably higher than the average frequency of the whole record. There were also two quiescent periods lasting over a century, namely the ones from 200 to 300 CE and 1000 to 1150 CE, with event frequency lower than 1.5 events/century.

4. Discussion

4.1. Modern TC event analog

Coastal karst basins are natural sediment traps recording paleo-environmental changes. During normal weather, their low-energy environments are less affected by external currents and waves due to the shelter of coral reefs or limestone walls, and therefore they tend to receive fine-grained carbonate clastics produced in adjacent lagoons and reefs (Gischler et al., 2008). The low oxygen environment at the bottom of a deep hole can inhibit bioturbation of the sediments.

The passage of a severe tropical cyclone around a basin brings high winds, and the resultant wave and storm surge raise water level and inundate the adjacent intertidal and supratidal zone. The extreme surface waves and currents significantly enhance the bottom shear stress on the reef and in the lagoon, leading to the entrainment and transport of relative coarser grains into the basin, which can be distinguished from the fine-grained depositions formed during normal quiescent conditions by visual inspection or coarse anomaly analysis.

Since 1964, at least 16 tropical cyclones passed within 150 km of the Bay of Islands. Among them, the strongest three were Meli (1979, category 4 on the Saffir-Simpson Scale, Taylor et al., 2021), Tomas (2010, category 4) and Winston (2016, category 5), whose passages probably instigated hydrodynamic conditions strong enough to leave coarse-grained depositions in the basin. Especially, Cyclone Winston whose center of circulation passed 10 km to the north of Bay of Islands when the storm had sustained winds in excess of 72 m/s (Fig. 4), and is estimated to be the most powerful and destructive storm on record having made landfall in Fiji (Fiji Meteorological Service, 2016; Terry and Lau, 2018). The associated wave height and flow velocities along Taveuni (Fig. 4) coasts reached over 10 m and 14 m/s, respectively, and quarried boulders from coral reefs and transported them onto the flats. According to the age model based on radiometric dating results, the upper most event bed was deposited between 2008 and 2017 CE. With Winston making landfall on Vanua Balavu at category 5 intensity, it is reasonable to infer that the event layer on the top of BOI2 (Fig. 3b) was left by this event; similarly, the second event layer dates 1988 to 2015 and thus we attribute this Tomas, which passed within 60 km of Vanua Balavu island in 2010 at peak category 4 intensity. The two modern TC events were used as chronologic markers to provide additional age control for BOI2 record due to their reliability.

The third event bed dates back between 1933 and 1959 CE, and thus occurs earlier than the other well documented severe TCs that passed further away from Vanua Balavu than Winston and Tomas in 2007 (Daman), 1985 (Eric), and 1979 (Meli). News reports indicate a severe cyclone impacted the Lau group (which includes Vanua Balavu) in December 1948 and the third event bed we identify was likely deposited during that event, though the precise track and intensity of this TC is unknown.

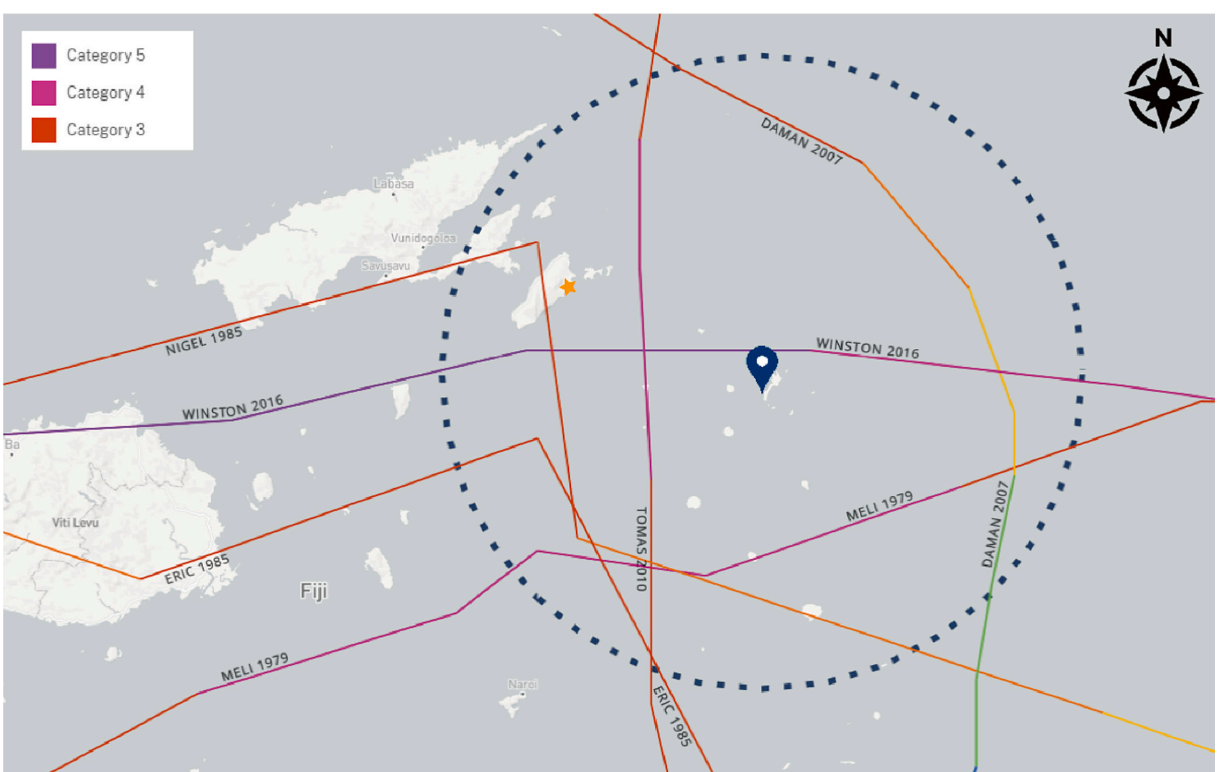

Fig. 4. Historical major tropical cyclone (category 3 and greater on the Saffir-Simpson Hurricane Scale) tracks (1964–2017) passing within 150 km of the karst basin in Bay of Islands (Data source: NOAA, 2024). The orange star indicates the study area of Terry and Lau (2018) in Taveuni Island.

Attempts have been made by previous studies to link sedimentary records found in various environments to TC-driven hydrodynamic variables. The magnitudes of high energy hydrodynamic conditions such as flow velocity and wave height have been calculated from boulder depositions (Nandasena et al., 2011; Goto et al., 2011; Hongo et al., 2018; Terry and Lau, 2018). Liu and Fearn (1993, 2000) suggested that the thickness, horizontal extent and shape of overwash sand layers preserved in coastal lakes are generally proportional to the hurricane intensity under stable geomorphic settings. Woodruff et al. (2008) applied a simple advective-settling inverse model to estimate the magnitudes of past flood events according to the lateral sorting pattern of overwash deposits in a lagoon. In general, it is promising to estimate the hydrodynamic variables that are responsible for the formation of TC event deposits under specific geomorphological and bathometric settings (Brandon et al., 2013; Lin et al., 2014). However, it is also notable that empirical formulas based on siliciclastic particles often generate remarkable errors when applied to predict the dynamic behaviors of carbonate grains due to their unusual shapes (Woodruff et al., 2008; Rieux et al., 2019; Li et al., 2020).

Nevertheless, the relationships between sediment transport, TC intensity and resultant hydrodynamics is complex. Firstly, the term TC intensity is merely a characteristic variable. For instance, the Saffir-Simpson Hurricane Wind Scale (Taylor et al., 2021) is based on the maximum sustained surface wind speed and it may not describe local conditions at a specific observing site. Moreover, storm size, translation speed, track and intensity work with bathymetry, topography, and vegetation cover to yield complicated patterns of sediment transport and deposition (Lin et al., 2014).

The category 5 Winston, category 4 Thomas and the TC in 1948 directly hit the site, therefore a proper cutoff threshold should identify their resultant event beds. Taking a 2-σ (corresponding to a 95 % probability) threshold will omit them, leaving only 12 events, while a 1-σ (68 %) threshold will bring in more minor peaks as event beds and the event number will rise to 53; eventually a 1.3-σ (80 %) threshold is adopted to balance. Given that the coarse fraction anomalies of Winston and Thomas are only moderate ones among all identified event beds, we are confident that that BOI2 has recorded intense storms comparative to them at least over the past 2000 years.

4.2. Comparison to other paleostorm records

The BOI2 record provides a local case of intense TC occurrence, while regional or basin-wide changes can be inferred by examining other paleostorm reconstructions in the Pacific basin. Concerning the data-point sparsity of Fitzsimons and Howarth (2022) in the recent two millenniums, the only available continuous paleostorm reconstruction in the SP basin is the lagoon sedimentary record from Tahaa Island provided by Toomey et al. (2013). It was reprocessed to form an event sequence using a similar data processing approach to BOI2. Several studies of beach ridges in northeastern Australia (Hayne and Chappell, 2001; Nott et al., 2009; Nott, 2011; Forsyth et al., 2010, 2012) are spatially clustered, but the dating results of the ridges in each study only partially overlap. Considering that each study area has specific sensitivity to different storm events due to its topography, source supply and hydrodynamic environment, combining the individual study sites into a total study area with a multiplicative increase in the total number of events should be able to provide a more comprehensive picture of the storm activity characteristics in this region. We chronologically ranked the years of beach ridges in each study and integrated them into a single time series by removing duplicates. In the North Pacific, the reconstruction from a coral reef lagoon deposition in Yongshu Reef, South China Sea was adopted.

As shown in Fig. 5, among the four paleostorm reconstructions, the BOI2 record provides the most continuous record and the highest event frequency (2.6 events/century). The overall frequencies of the other three records are lower (less than 2 events/century), and there are some gaps (without any TC occurrence) lasting for decades. Variations in event frequency and continuity is partly a reflection of the number of TC passing within range of a study site, while on the other hand, it can be attributed to site sensitivity, geographical and geological settings, and stochastic processes associated with TC tracks and landfall locations (Wallace et al., 2021).

Coherent intense TC activity patterns on multi-centennial scale are found between different sites. Yongshu Reef record and Australian beach ridges show very similar trends prior to 800 CE and after 1200 CE. Especially, within the three centuries from 1600 to 1900 CE, all the four paleostorm records saw a rise in TC occurrence, while their paces are not consistent. Taken together, the four different reconstructions spanning over wide temporal and spatial scales suggest intervals of heightened intense TC activity and imply underlying forcings.

4.3. Climate forcing of TC activity in the South Pacific

Tropical cyclones tend to develop in regions where four essential background conditions are present: adequate thermodynamic energy containing in a warm ocean surface layer, sufficient moisture in the atmosphere, low-level relative cyclonic vorticity and minimal vertical wind shear around (Gray, 1979; Widlansky et al., 2019). In the Pacific basin, the Intertropical Convergence Zone (ITCZ) and SPCZ meet these requirements and are the main development region of tropical cyclones (MDR).

Climate modes and basin internal forcings are the primary factors controlling the temporal and spatial characteristics of cyclone genesis and development. Temperature variability is the principal index of global climate change; in the past two thousand years, the Medieval Climate Anomaly (MCA) and the Little Ice Age (LIA) are two well-known climatic intervals that appear to have driven changes in TC occurrence elsewhere (Bramante et al., 2020; Minamidate and Goto, 2024). MCA, a phase of warming mostly observed in the North Atlantic Ocean, extended from the 9th to the 13th centuries, while the LIA was a time of lower temperatures that spanned from the 13th to the 19th centuries, predominantly affecting Europe, although its effects were also noted in regions beyond Europe (Mann et al., 2009). Though the hydroclimatic proxies often suggest synchronous changes, the length and extent of MCA and LIA exhibited variabilities across different regions and times rather than uniform epochs on a global scale. Continental-scaled temperature reconstructions (Ahmed et al., 2013; Fig. 5*h*) show that MCA and LIA started later and spanned shorter in the Australasia than the North Hemisphere continents.

ENSO is one of the most significant global climate modes, and prominent La Niña events have been detected during LIA (Emile-Geay et al., 2013; Fig. 5*g*). ENSO is usually acknowledged as the dominant climate mode controlling typhoon genesis locations, tracks and their likelihood of making landfall. For example, in the western North Pacific, Elsner and Liu (2003) carried out a cluster analysis on modern instrumental typhoon data and classified typhoon tracks into three general types: straight-moving (SM), recurving (RC) and north-oriented (NO) tracks. Among the three track categories, a significant negative correlation between the annual numbers of straight-moving and recurving typhoons was detected (Liu et al., 2001; Elsner and Liu, 2003). Moreover, during La Niña years, more typhoons make their landfalls over southern China along the SM path while during El Niño years more typhoons favor the RC path, which is corroborated by instrumental data (Lander, 1994; Elsner and Liu, 2003), historical typhoon records (Liu et al., 2001; Elsner and Liu, 2003), typhoon reconstructions based on sedimentological and geochemical proxies (Woodruff et al., 2009; Yu et al., 2009; Katsuki et al., 2016; Katsuki et al., 2017; Zhou et al., 2019; Yue et al., 2019) and reconstructed ENSO indices (Cook et al., 2000).

Observations and reconstructions suggest that ENSO displaces the position of ITCZ latitudinally (Thompson et al., 2013) and changes the climatic conditions favoring TC genesis and intensification (Bramante et al., 2020); it also dominates the phase of Western Pacific Warm Pool

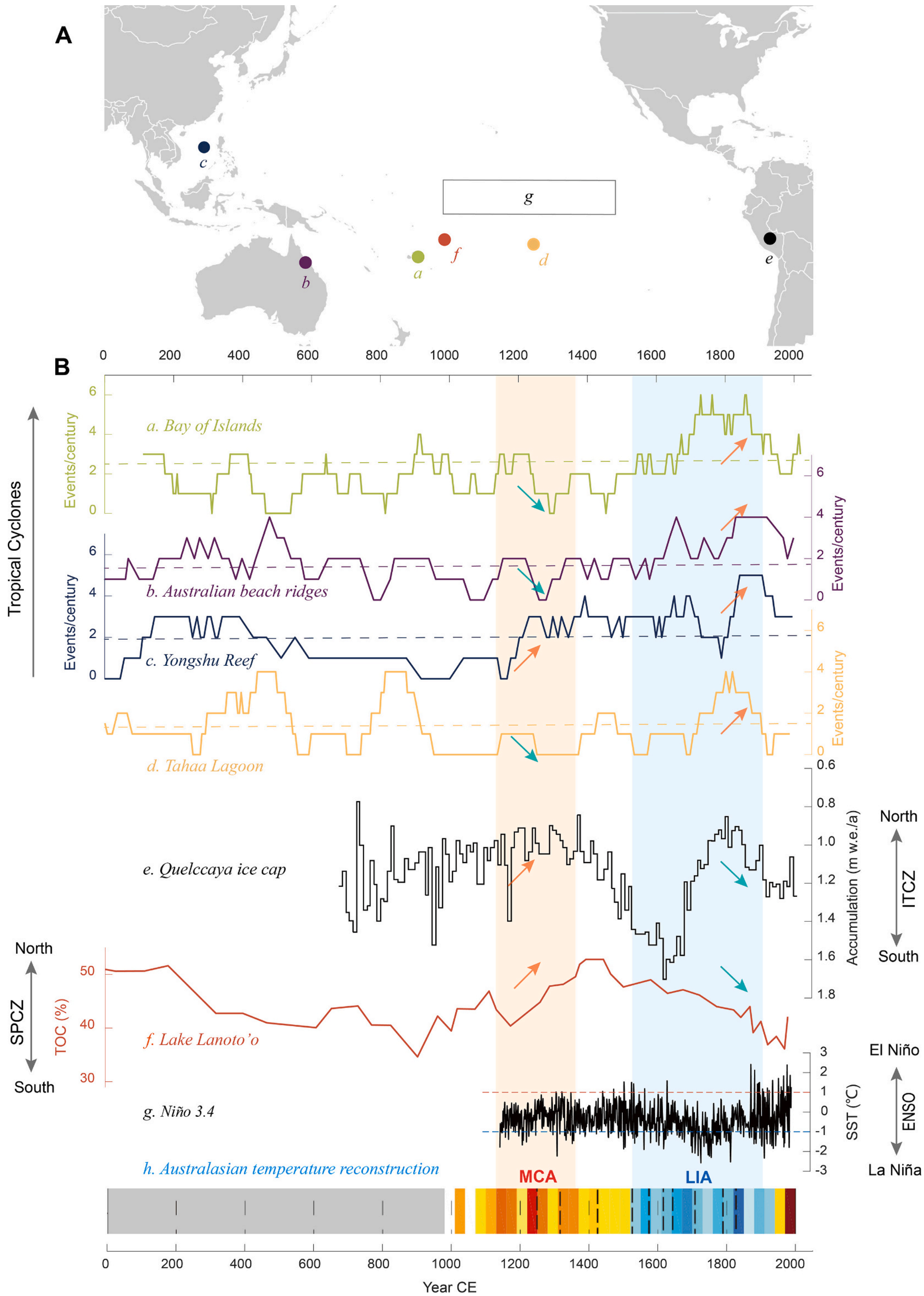

Fig. 5. Paleoclimate and paleostorm reconstructions in the past 2000 years for the Pacific basin. (A) Regional map of the Pacific Basin, with lowercases showing the site positions of the records used below. (B) Paleoclimate and paleostorm reconstructions in the Pacific basin: (*a*) Paleostorm reconstruction from a karst basin record, Bay of Islands, Vanua Balavu, Fiji (this study); (*b*) Paleostorm reconstruction by integrating beach ridge results in the northeast Australian coasts (data sources: Hayne and Chappell, 2001; Nott et al., 2009; Nott, 2011; Forsyth et al., 2010; Forsyth et al., 2012); (*c*) Paleostorm reconstruction from a coral reef lagoon deposition in Yongshu Reef, South China Sea (data source: Yu et al., 2009); (*d*) Paleostorm reconstruction from a lagoon deposition in Tahaa, French Polynesia (data source: Toomey et al., 2013); (*e*) Net accumulation rate of $\delta^{18}O$ reconstructed from ice cores of Quelccaya, Peru (data source: Thompson et al., 2013); (*f*) Total organic carbon (TOC) reconstructed from Lake Lanoto'o, Samoa, data source: Hassall (2017); (*g*) Reconstruction of central equatorial pacific SST variability over the past millennium (data source: Emile-Geay et al., 2013); (*h*) Continental-scaled temperature reconstructions of Australasia, modified from Ahmed et al. (2013). Subfigure *a* - *d* are expressed in terms of event frequency (event number in the past century), wherein dashed lines present the overall average event frequencies of corresponding records.

(Wu et al., 2013) and steering flows, and consequently affect TC tracks. Fig. 5*e* indicates remarkable southward shifts of ITCZ at the beginning of LIA with more La Niña events presenting in Fig. 5*g*, and a synchronous TC frequency rise occurs in the South China Sea (Fig. 5*c*). Bramante et al. (2020) as well reported frequent storms in the North Pacific during early LIA, and they attributed the enhanced TC activity to the migration of Pacific Walker Circulation, and the variations of ENSO and Pacific Meridional Mode; such mechanisms probably underlie the tropical cyclone raise in the LIA in the SP as well. During 1700 to 1850 CE, the ITCZ saw northward displacements, accompanied by decreased TC landfalls in the South China Sea and increased La Niña events. It seems that it is not appropriate to use a simple ENSO index to characterize TC variability in the North Pacific region.

In the SP, the SPCZ creates large-scale atmospheric conditions that favor TC genesis during the austral summer, making it the peak of regional TC season (Brown et al., 2020). Instrumental records and reconstructions indicate that SPCZ diagonal axis is displaced from its climatological position by different phases and interannual variations of the ENSO cycle through variability of the western/central Pacific equatorial sea surface temperature (Basher and Zheng, 1995; Kuleshov et al., 2008; Ramsay et al., 2008). Specifically, during El Niño events, the SPCZ shifts north-east, closer to the equator, whereas during La Niña events, it moves south-west and poleward. The SPCZ displacements modulate the atmospheric circulation in the SP and consequently drive TC genesis and track variabilities in this region (Jourdain et al., 2011; Vincent et al., 2011; Menkes et al., 2012). The analysis of Vincent et al. (2011) suggests that the north-eastward displacement of SPCZ during La Niña events induces increasement of cyclogenesis near Fiji and permits tropical cyclones to track farther westwards of their usual positions, and vice versa.

Hassall (2017) reveals a persistent southward shift (expansion) of SPCZ through the whole LIA using TOC records from Lake Lanoto'o, a freshwater lake of Samoa, and a northward movement (contraction) of SPCZ during MCA (Fig. 5*f*), corresponding to the sustained eastward shift of SPCZ during MCA suggested by Higgins et al. (2020) based on a trans-Pacific tree-ring network. The reconstructions from the lagoon of Tahaa, Bay of Islands and Australian beach ridges (Fig. 5*a, b & d*) present subaverage overall event frequencies during MCA, while their response to the southward SPCZ displacement through LIA are slightly different, despite of general increasing trends. Tahaa is located near the diagonal axis of SPCZ, and the other two sites are basically aligned along the southwestern edge, while their peaks of TC frequency during the LIA present a latitudinal lag from west to east. It calls for more high resolution paleostorm reconstructions in this basin and evidence from global climate models to clarify whether it is a general scenario driven by temporal and spatial variabilities of SPCZ and other climate forcings, or it is merely a phenomenon induced by stochastic processes, site sensitivity, and data analysis uncertainty etc.

Apart from the diagonally oriented axis, the SPCZ has a zonal axis located over the West Pacific Warm Pool, where it meets the ITCZ (Vincent, 1994). This could probably explain the intriguing fact that the Australian beach ridge record and the Yongshu Reef record show very similar patterns during MCA and LIA. TC activity near the northeast Australian coast is probably subject to combined effects of the diagonal and zonal axes of SPCZ, and the latter is closely associated with the ITCZ.

5. Conclusions

In this paper, a sedimentary record (BOI2) from a karst basin in Bay of Islands, Vanua Balavu, Fiji, is presented, which provides insight into the history of intense tropical cyclone activity in the past 2000 years in the central SP.

Coarse fraction (>63 μm) anomalies in the BOI2 core are used as the main proxy of intense TC events, and 53 storm events captured by this site are identified, suggesting an overall average event frequency of 2.6 events/century. This reconstruction features multiple centennial-scale quiescent periods (from 200 to 300 CE and 1000 to 1150 CE) and active periods (namely from 350 to 750 CE, 900 to 1000 CE, 1150 to 1250 CE, 1400 to 1500 CE, and 1650 to 2017 CE), and the most frequent interval spanned from 1650 to 1800 CE at 4.5 events/century.

A comparison between existing paleostorm records and climate forcing indices suggests that the SPCZ provides conditions favoring cyclogenesis and intensification. SPCZ's southward displacement during the Little Ice Age with more La Niña events is responsible for the extensive increasing of TC activity in the SP basin, corresponding to synchronous active typhoon activity in the South China Sea. Decline of TC occurrence in the western SP during the Medieval Climate Anomaly is attributed to the northward movement of SPCZ.

However, event frequency peaks of the latitudinally aligned sites in the SP exhibit a certain degree of asynchrony, calling for more high resolution paleostorm reconstructions in this basin and evidence from global climate models to achieve more general conclusions.

CRediT authorship contribution statement

Yanan Li: Writing – review & editing, Writing – original draft, Methodology, Investigation, Formal analysis, Conceptualization. **Jeffrey P. Donnelly:** Writing – review & editing, Validation, Supervision, Project administration, Investigation, Funding acquisition, Conceptualization. **Nicole d'Entremont:** Methodology, Investigation. **James F. Bramante:** Methodology, Investigation. **Krishna K. Kotra:** Methodology, Investigation. **Shu Gao:** Writing – review & editing, Validation.

Declaration of competing interest

The authors declare the following financial interests/personal relationships which may be considered as potential competing interests: Yanan Li reports financial support was provided by China Postdoctoral Science Foundation. Shu Gao reports financial support was provided by National Natural Science Foundation of China. If there are other authors, they declare that they have no known competing financial interests or personal relationships that could have appeared to influence the work reported in this paper.

Acknowledgement

This study was funded by the China Postdoctoral Science Foundation (2023M731588) and the National Natural Science Foundation of China (41530962, 42076172). The authors thank Kelly McKeon for providing lab skill training, and Dr. Elizabeth J. Wallace for improving the data analysis algorithms.

Appendix A. Supplementary data

Supplementary data to this article can be found online at https://doi.org/10.1016/j.palaeo.2025.113090.

Data availability

Data will be made available on request.

References

Ahmed, M., Anchukaitis, K.J., Asrat, A., Borgaonkar, H.P., Braida, M., Buckley, B.M., et al., 2013. Continental-scale temperature variability during the past two millennia. Nat. Geosci. 6 (5), 339–346.
Basher, R.E., Zheng, X., 1995. Tropical Cyclones in the Southwest Pacific: Spatial patterns and Relationships to Southern Oscillation and Sea Surface Temperature. J. Clim. 8 (5), 1249–1260.
Blaauw, M., Christen, J.A., 2011. Flexible paleoclimate age-depth models using an autoregressive gamma process. Bayesian Anal. 6 (3), 457–474.
Bramante, J.F., Ford, M.R., Kench, P.S., Ashton, A.D., Toomey, M.R., Sullivan, R.M., et al., 2020. Increased typhoon activity in the Pacific deep tropics driven by Little Ice Age circulation changes. Nat. Geosci. 13 (12), 806–811.

Brandon, C.M., Woodruff, J.D., Lane, D., Donnelly, J.P., 2013. Tropical cyclone wind speed constraints from resultant storm surge deposition: a 2500 year reconstruction of hurricane activity from St. Marks, FL. Geochem. Geophys. Geosyst. 14 (8), 2993–3008.
Brown, J.R., Lengaigne, M., Lintner, B.R., Widlansky, M.J., van der Wiel, K., Dutheil, C., et al., 2020. South Pacific Convergence Zone dynamics, variability and impacts in a changing climate. Nat. Rev. Earth Environ. 1 (10), 530–543.
Cook, E., Buckley, B., D'arrigo, R., Peterson, M., 2000. Warm-season temperatures since 1600 BC reconstructed from Tasmanian tree rings and their relationship to large-scale sea surface temperature anomalies. Clim. Dyn. 16, 79–91.
Denniston, R.F., Villarini, G., Gonzales, A.N., Wyrwoll, K.-H., Polyak, V.J., Ummenhofer, C.C., et al., 2015. Extreme rainfall activity in the Australian tropics reflects changes in the El Niño/Southern Oscillation over the last two millennia. Proc. Natl. Acad. Sci. 112 (15), 4576–4581.
Denommee, K.C., Bentley, S.J., Droxler, A.W., 2014. Climatic controls on hurricane patterns: a 1200-y near-annual record from Lighthouse Reef, Belize. Sci. Rep. 4 (1), 3876.
Donnelly, J.P., 2005. Evidence of past intense tropical cyclones from backbarrier salt pond sediments: a case study from Isla de Culebrita, Puerto Rico, USA. J. Coast. Res. 201–210.
Donnelly, J.P., Woodruff, J.D., 2007. Intense hurricane activity over the past 5,000 years controlled by El Niño and the West African monsoon. Nature 447 (7143), 465.
Donnelly, J.P., Bryant, S.S., Butler, J., Dowling, J., Fan, L., Hausmann, N., et al., 2001a. 700 yr sedimentary record of intense hurricane landfalls in southern New England. GSA Bull. 113 (6), 714–727.
Donnelly, J.P., Roll, S., Wengren, M., Butler, J., Lederer, R., Webb Iii, T., 2001b. Sedimentary evidence of intense hurricane strikes from New Jersey. Geology 29 (7), 615–618.
Donnelly, J.P., Hawkes, A.D., Lane, P., MacDonald, D., Shuman, B.N., Toomey, M.R., et al., 2015. Climate forcing of unprecedented intense-hurricane activity in the last 2000 years. Earth's Future 3 (2), 49–65.
Elsner, J.B., Liu, K.B., 2003. Examining the ENSO-typhoon hypothesis. Clim. Res. 25 (1), 43–54.
Emery, K.O., 1969. A Coastal Pond Studied by Oceanographic Methods. Elsevier, New York, 82 pp.
Emile-Geay, J., Cobb, K.M., Mann, M.E., Wittenberg, A.T., 2013. Estimating Central Equatorial Pacific SST Variability over the Past Millennium. Part II: Reconstructions and Implications. J. Clim. 26 (7), 2329–2352.
Fiji Meteorological Service, 2016. 2015 Annual Climate Summary. Retrieved from. http://www.met.gov.fj/Summary2.pdf.
Fitzsimons, S., Howarth, J., 2022. Developing lacustrine sedimentary records of storminess in southwestern New Zealand. Quat. Sci. Rev. 277, 107355.
Forsyth, A.J., Nott, J., Bateman, M.D., 2010. Beach ridge plain evidence of a variable late-Holocene tropical cyclone climate, North Queensland, Australia. Palaeogeogr. Palaeoclimatol. Palaeoecol. 297 (3), 707–716.
Forsyth, A.J., Nott, J., Bateman, M.D., Beaman, R.J., 2012. Juxtaposed beach ridges and foredunes within a ridge plain — Wonga Beach, Northeast Australia. Mar. Geol. 307-310, 111–116.
Gassner, P., Yakub, N., Kaitu'u, J., Wendt, H., West-erveld, L., Macmillan-Lawler, M., et al., 2019. Marine Atlas. Maximizing Benefits for Fiji. In: MACBIO (GIZ/IUCN/SPREP): Suva, Fiji.
Gill, J.B., 1976. From island arc to oceanic islands: Fiji, southwestern Pacific. Geology 4 (2), 123–126.
Gischler, E., Shinn, E.A., Oschmann, W., Fiebig, J., Buster, N.A., 2008. A 1500-Year Holocene Caribbean climate Archive from the Blue Hole, Lighthouse Reef, Belize. J. Coast. Res. 2008 (246), 1495–1505, 1411.
Gooley, G., Abbs, D., Grose, M., Hemer, M., Lenton, A., Zhang, X., et al., 2014. Climate Variability, Extremes and Change in the Western Tropical Pacific: New Science and Updated Country Reports, 2014. CSIRO and Australian Bureau of Meteorology, Melbourne.
Goto, K., Miyagi, K., Kawana, T., Takahashi, J., Imamura, F., 2011. Emplacement and movement of boulders by known storm waves—field evidence from the Okinawa Islands, Japan. Mar. Geol. 283 (1–4), 66–78.
Gray, W., 1979. Hurricanes: their formation, structure and likely role in the tropical circulation. Meteorol. Trop. Oceans 155–218.
Hassall, J.D., 2017. Static or Dynamic: Reconstructing Past Movement of the South Pacific Convergence Zone. University of Southampton.
Hayne, M., Chappell, J., 2001. Cyclone frequency during the last 5000 years at Curacoa Island, North Queensland, Australia. Palaeogeogr. Palaeoclimatol. Palaeoecol. 168 (3), 207–219.
Higgins, P.A., Palmer, J.G., Turney, C.S.M., Andersen, M.S., Cook, E.R., 2020. One Thousand three Hundred Years of Variability in the Position of the South Pacific Convergence Zone. Geophys. Res. Lett. 47 (17) e2020GL088238.
Hogg, A.G., Hua, Q., Blackwell, P.G., Niu, M., Buck, C.E., Guilderson, T.P., et al., 2013. SHCal13 Southern Hemisphere calibration, 0–50,000 years cal BP. Radiocarbon 55 (4), 1889–1903.
Hongo, C., Kurihara, H., Golbuu, Y., 2018. Coral boulders on Melekeok reef in the Palau Islands: an indicator of wave activity associated with tropical cyclones. Mar. Geol. 399, 14–22.
Huang, G., 2000. Holocene Record of Storms in Sediments of the Pearl River Estuary and Vicinity. Hongkong University.
Jourdain, N.C., Marchesiello, P., Menkes, C.E., Lefèvre, J., Vincent, E.M., Lengaigne, M., Chauvin, F., 2011. Mesoscale simulation of Tropical Cyclones in the South Pacific: Climatology and Interannual Variability. J. Clim. 24 (1), 3–25.
Katsuki, K., Yang, D.-Y., Seto, K., Yasuhara, M., Takata, H., Otsuka, M., et al., 2016. Factors controlling typhoons and storm rain on the Korean Peninsula during the Little Ice Age. J. Paleolimnol. 55 (1), 35–48.
Katsuki, K., Yang, D.-Y., Lim, J., Lee, J.-Y., Asahi, H., Han, M., 2017. Multi-centennial-scale changes in East Asian typhoon frequency during the mid-Holocene. Palaeogeogr. Palaeoclimatol. Palaeoecol. 476, 140–146.
Kuleshov, Y., Qi, L., Fawcett, R., Jones, D., 2008. On tropical cyclone activity in the Southern Hemisphere: Trends and the ENSO connection. Geophys. Res. Lett. 35 (14).
Kumar, R., 2005. Geology, climate, and landscape of the PABITRA wet-zone transect, Viti Levu Island, Fiji. Pac. Sci. 59 (2), 141–157.
Lander, M.A., 1994. An exploratory analysis of the relationship between tropical storm formation in the western North Pacific and ENSO. Mon. Weather Rev. 122 (4), 636–651.
Lane, P., Donnelly, J.P., Woodruff, J.D., Hawkes, A.D., 2011. A decadally-resolved paleohurricane record archived in the late Holocene sediments of a Florida sinkhole. Mar. Geol. 287 (1–4), 14–30.
Leslie, D.M., Blakemore, L.C., 1985. Properties and classification of selected soils from Vanua Balavu, Lau Group, Fiji. J. R. Soc. N. Z. 15 (3), 313–327.
Li, Y., Yu, Q., Gao, S., Flemming, B.W., 2020. Settling velocity and drag coefficient of platy shell fragments. Sedimentology 67 (4), 2095–2110.
Lin, N., Lane, P., Emanuel, K.A., Sullivan, R.M., Donnelly, J.P., 2014. Heightened hurricane surge risk in Northwest Florida revealed from climatological-hydrodynamic modeling and paleorecord reconstruction. J. Geophys. Res. Atmos. 119 (14), 8606–8623.
Liu, K.-B., Fearn, M.L., 1993. Lake-sediment record of late Holocene hurricane activities from coastal Alabama. Geology 21 (9), 793–796.
Liu, K.-B., Fearn, M.L., 2000. Reconstruction of prehistoric landfall frequencies of catastrophic hurricanes in northwestern Florida from lake sediment records. Quat. Res. 54 (2), 238–245.
Liu, K.-B., Shen, C., Louie, K.-S., 2001. A 1,000-year history of Typhoon Landfalls in Guangdong, Southern China, Reconstructed from Chinese Historical Documentary Records. Ann. Assoc. Am. Geogr. 91 (3), 453–464.
Mann, M.E., Zhang, Z., Rutherford, S., Bradley, R.S., Hughes, M.K., Shindell, D., et al., 2009. Global Signatures and Dynamical Origins of the Little Ice Age and medieval climate Anomaly. Science 326 (5957), 1256–1260.
Menkes, C.E., Lengaigne, M., Marchesiello, P., Jourdain, N.C., Vincent, E.M., Lefèvre, J., et al., 2012. Comparison of tropical cyclogenesis indices on seasonal to interannual timescales. Clim. Dyn. 38 (1), 301–321.
Minamidate, K., Goto, K., 2024. Unveiling the history and nature of paleostorms in the Holocene. Earth Sci. Rev. 253, 104774.
Nandasena, N.A.K., Paris, R., Tanaka, N., 2011. Reassessment of hydrodynamic equations: minimum flow velocity to initiate boulder transport by high energy events (storms, tsunamis). Mar. Geol. 281 (1–4), 70–84.
Neall, V.E., Trewick, S.A., 2008. The age and origin of the Pacific islands: a geological overview. Philos. Trans. R. Soc. B 363 (1508), 3293–3308.
Nott, J., 2006. Tropical cyclones and the evolution of the sedimentary coast of northern Australia. J. Coast. Res. 49–62.
Nott, J., 2011. A 6000 year tropical cyclone record from Western Australia. Quat. Sci. Rev. 30 (5–6), 713–722.
Nott, J., Smithers, S., Walsh, K., Rhodes, E., 2009. Sand beach ridges record 6000 year history of extreme tropical cyclone activity in northeastern Australia. Quat. Sci. Rev. 28 (15–16), 1511–1520.
Nunn, P.D., Ollier, C., Hope, G., Rodda, P., Omura, A., Peltier, W.R., 2002. Late Quaternary Sea-level and tectonic changes in Northeast Fiji. Mar. Geol. 187 (3), 299–311.
PACCSAP, 2015. Current and future climate of the Fiji Islands. Retrieved from. https://www.pacificclimatechangescience.org/wp-content/uploads/2013/06/1_PACCSAP-Fiji-11pp_WEB.pdf.
Ramsay, H.A., Leslie, L.M., Lamb, P.J., Richman, M.B., Leplastrier, M., 2008. Interannual Variability of Tropical Cyclones in the Australian Region: Role of Large-Scale Environment. J. Clim. 21 (5), 1083–1103.
Rieux, A., Weill, P., Mouaze, D., Poirier, C., Nechenache, F., Perez, L., Tessier, B., 2019. Threshold of motion and settling velocities of mollusc shell debris: Influence of faunal composition. Sedimentology 66 (3), 895–916.
Tan, F., Zhang, Y., Cao, L., Xu, H., Shi, Q., Zhang, X., et al., 2023. Meridional response of Western North Pacific paleocyclone activity to tropical atmospheric circulation variability over the past millennium. Palaeogeogr. Palaeoclimatol. Palaeoecol. 610, 111331.
Taylor, H.T., Ward, B., Willis, M., Zaleski, W., 2021. The Saffir-Simpson Hurricane Wind Scale. Retrieved from. https://www.nhc.noaa.gov/pdf/sshws.pdf.
Terry, J.P., Lau, A.Y.A., 2018. Magnitudes of nearshore waves generated by tropical cyclone Winston, the strongest landfalling cyclone in South Pacific records. Unprecedented or unremarkable? Sediment. Geol. 364, 276–285.
Thompson, L.G., Mosley-Thompson, E., Davis, M.E., Zagorodnov, V.S., Howat, I.M., Mikhalenko, V.N., Lin, P.-N., 2013. Annually Resolved Ice Core Records of Tropical Climate Variability over the past ~1800 years. Science 340 (6135), 945–950.
Toomey, M.R., Curry, W.B., Donnelly, J.P., van Hengstum, P.J., 2013. Reconstructing 7000 years of North Atlantic hurricane variability using deep-sea sediment cores from the western Great Bahama Bank. Paleoceanography 28 (1), 31–41.
Vincent, D.G., 1994. The South Pacific convergence zone (SPCZ): a review. Mon. Weather Rev. 122 (9), 1949–1970.
Vincent, E.M., Lengaigne, M., Menkes, C.E., Jourdain, N.C., Marchesiello, P., Madec, G., 2011. Interannual variability of the South Pacific Convergence Zone and implications for tropical cyclone genesis. Clim. Dyn. 36 (9), 1881–1896.
Wallace, D.J., Woodruff, J.D., Anderson, J.B., Donnelly, J.P., 2014. Palaeohurricane reconstructions from sedimentary archives along the Gulf of Mexico, Caribbean Sea

and western North Atlantic Ocean margins. Geol. Soc. Lond. Spec. Publ. 388, SP388–312.
Wallace, E.J., Donnelly, J.P., van Hengstum, P.J., Wiman, C., Sullivan, R.M., Winkler, T. S., et al., 2019. Intense hurricane activity over the past 1500 years at South Andros Island, The Bahamas. Paleoceanogr. Paleoclimatol. 36 (11), 1761–1783.
Wallace, E.J., Donnelly, J.P., Van Hengstum, P.J., Winkler, T.S., McKeon, K., Macdonald, D., et al., 2021. 1050 years of hurricane strikes on Long Island in the Bahamas. Paleoceanogr. Paleoclimatol. 36 (3).
Widlansky, M.J., Annamalai, H., Gingerich, S.B., Storlazzi, C.D., Marra, J.J., Hodges, K.I., et al., 2019. Tropical Cyclone Projections: changing climate Threats for Pacific Island Defense Installations. Weather Climate Soc. 11 (1), 3–15.
Williams, H., Choowong, M., Phantuwongraj, S., Surakietchai, P., Thongkhao, T., Kongsen, S., Simon, E., 2016. Geologic records of Holocene typhoon strikes on the Gulf of Thailand coast. Mar. Geol. 372, 66–78.
Woodruff, J.D., Donnelly, J.P., Mohrig, D., Geyer, W.R., 2008. Reconstructing relative flooding intensities responsible for hurricane-induced deposits from Laguna Playa Grande, Vieques, Puerto Rico. Geology 36 (5), 391–394.
Woodruff, J.D., Donnelly, J.P., Okusu, A., 2009. Exploring typhoon variability over the mid-to-late Holocene: evidence of extreme coastal flooding from Kamikoshiki, Japan. Quat. Sci. Rev. 28 (17–18), 1774–1785.
Wu, H.C., Linsley, B.K., Dassié, E.P., Schiraldi, B., deMenocal, P.B., 2013. Oceanographic variability in the South Pacific Convergence Zone region over the last 210 years from multi-site coral Sr/ca records. Geochem. Geophys. Geosyst. 14 (5), 1435–1453.
Yang, Y., Piper, D.J.W., Xu, M., Gao, J., Jia, J., Normandeau, A., et al., 2022. Northwestern Pacific tropical cyclone activity enhanced by increased Asian dust emissions during the Little Ice Age. Nat. Commun. 13 (1), 1712.
Yu, K.-F., Zhao, J.-X., Shi, Q., Meng, Q.-S., 2009. Reconstruction of storm/tsunami records over the last 4000 years using transported coral blocks and lagoon sediments in the southern South China Sea. Quat. Int. 195 (1–2), 128–137.
Yu, K., Zhao, J., Roff, G., Lybolt, M., Feng, Y., Clark, T., Li, S., 2012. High-precision U-series ages of transported coral blocks on Heron Reef (southern Great Barrier Reef) and storm activity during the past century. Palaeogeogr. Palaeoclimatol. Palaeoecol. 337 (Supplement C), 23–36.
Yue, Y., Yu, K., Tao, S., Zhang, H., Liu, G., Wang, N., et al., 2019. 3500-year western Pacific storm record warns of additional storm activity in a warming warm pool. Palaeogeogr. Palaeoclimatol. Palaeoecol. 521, 57–71.
Zhou, L., Yang, Y., Wang, Z., Jia, J., Mao, L., Li, Z., et al., 2019. Investigating ENSO and WPWP modulated typhoon variability in the South China Sea during the mid–late Holocene using sedimentological evidence from southeastern Hainan Island, China. Mar. Geol. 105987.